

# Clinical Validations on Effective Skin Clutter Rejection for Microwave Breast Cancer Diagnosis

Ayumi Ueda and Shouhei Kidera , Senior Member, IEEE

**Abstract**—This paper presents a cancer recognition scheme based on backscattered raw data using effective surface clutter rejection in microwave breast cancer diagnosis. Microwave breast cancer diagnostics enables a non-ionizing, non-compressive, low-cost examination, which can enhance the examination rate and frequency. A traditional radar image based cancer diagnosis faces a critical difficulty in discriminating cancer in highly dense breasts due to low contrast from fibro-glandular tissues. Therefore, this study introduces a direct recognition scheme from a complex-valued scattered signal, without using any imaging process, in which an efficient skin surface reflection (SSR) approach is introduced. Clinical data from over 100 Japanese subjects show that our SSR approach can enhance the recognition rate of cancerous tissues via a support vector machine (SVM) based learning approach.

**Index Terms**—Microwave breast cancer diagnosis, radar imaging, machine learning, skin surface reflection (SSR), clinical data validation.

## I. INTRODUCTION

ACCORDING to global statistics from the World Cancer Research Foundation, breast cancer is the most commonly diagnosed and fatal cancer worldwide [1]. X-ray imaging remains the most widely used screening tool; however, it involves significant X-ray exposure that can harm healthy tissue, and necessitates a painful breast compression during the procedure. These factors result in a lower examination rate, particularly among young women. While magnetic resonance imaging (MRI) offers safe, high-resolution imaging, it requires large, expensive equipment for electric and magnetic shielding. Ultrasound-based diagnosis, though safe and non-invasive, has limitations, as its recognition accuracy largely depends on the skill and experience of the operator. Additionally, in dense breasts, it often results in a high false-positive rate due to the difficulty in distinguishing between fibro-glandular and cancerous tissues. On the contrary, low-energy microwave screening provides significant advantages in terms of safety, affordability,

compactness, and non-contact measurement [2], [3], which is a crucial factor in improving screening rates. These features also enable more frequent examinations, which can lead to earlier detection of breast cancer and, consequently, better outcomes.

Several studies and ex-vivo investigations have demonstrated a distinct dielectric contrast between normal adipose tissue and tumor tissues [4], which has fueled the development of microwave-based cancer detection methods. Over the past few decades, numerous clinical studies have explored the use of microwave imaging for breast cancer detection [5], [6], [7], [8], [9], demonstrating variations in dielectric properties due to breast variability [10] and evaluating the sensitivity and specificity across numerous subjects [11], [12]. There are two primary approaches for image analysis of microwave scattered data to identify cancerous tissue. One approach is coherent integration (CI)-based imaging, commonly referred to as con-focal imaging, beamforming, or modified delay-and-sum methods [13], [14], [15], [16]. However, CI based imaging suffers from a high false-positive rate because it offers only a qualitative spatial profile of the reflection coefficient. In dense breasts, fibroglandular tissue surrounded by adipose area (with lower permittivity) can produce a strong response that hinders cancer detection. The other approach, inverse scattering (IS) analysis, also known as the tomography approach, offers a quantitative dielectric profile by solving the domain integral equation. Since the IS problem is nonlinear and generally ill-conditioned, various techniques such as the Born approximations, the distorted Born iterative method (DBIM) [17], [18], [19], [20], [21] and contrast source based inversion (CSI) [22], [23], [24] have been developed. While these methods provide a more accurate reconstruction of cancerous tissue, even in highly dense breasts, they are computationally intensive, particularly in three-dimensional imaging scenarios.

Building on the aforementioned background, we focused on the backscattered echo-based recognition method using a machine learning strategy, enhanced by an advanced skin surface reflection (SSR) scheme. While numerous studies have utilized the microwave band for breast cancer detection, they often rely on specific imaging techniques, such as radar or tomography, to generate input data for machine learning. Consequently, the recognition performance in these studies is highly dependent on the spatial resolution or reconstruction accuracy of the selected imaging method or condition, although several such studies have been published [25], [26], [27], [28], [29], [30], [31]. To address the above-mentioned issue, this study omits the intermediate imaging step, and instead directly inputs matched-filtered

Received 6 December 2024; revised 27 February 2025 and 3 April 2025; accepted 15 April 2025. This work was supported in part by JSPS KAKENHI under Grant JP23K26113 and in part by Asahi Glass Foundation, Continuation Grants for Young Researchers. (Corresponding author: Shouhei Kidera.)

This work involved human subjects or animals in its research. Approval of all ethical and experimental procedures and protocols was granted by the Certified Review Board of the Hiroshima University Hospital under Application No. CRB6180006.

The authors are with the Graduate School of Informatics and Engineering, The University of Electro-Communications, Tokyo 182-8585, Japan (e-mail: kidera@uec.ac.jp).

Digital Object Identifier 10.1109/JERM.2025.3562571

backscattered data into the machine learning process. While some studies [32] introduced supervised machine learning approaches for breast cancer detection or characterization, most of them assumed unrealistic breast models, such as non-dispersive or homogeneous media. Furthermore, as another novel aspect of our study, we introduce a cutting-edge SSR technique based on the fractional derivative (FD) model [33], aimed at improving the backscattered signal-based learning scheme. While there are numerous SSR approaches in the literature, such as FIR [16], singular value decomposition (SVD) [34], entropy-based time windowing [35], and two-stage processing [36], this FD-based SSR method optimizes the FD parameter to account for the frequency dependence of the skin surface reflection waveform. This optimization significantly reduces skin clutter signals, particularly when mutual coupling effects between the antenna and skin occur. Additionally, we incorporate simple averaging (SA) or singular value decomposition (SVD)-based data compression for a rotating measurement model, which provides a low-dimensional input vector and enhances noise suppression.

Furthermore, this study includes a large-scale clinical trial involving more than 100 cases, both cancerous and non-cancerous cases, conducted at Hiroshima University Hospital in 2019, utilizing multiple-input multiple-output (MIMO) ultrawide band radar equipment [15]. We begin by introducing and validating the effectiveness of the SSR method using the FD model, and investigate the performance of support vector machine (SVM)-based cancer recognition using the clinical datasets.

The main contributions of this study are summarized as:

- 1) Backscattered data based cancer recognition scheme by SVM based supervised machine learning is introduced, where no imaging processing is required. To reduce the dimension of the input vectors for the post-SVM process, the rotation augmented data are compressed by SVD process.
- 2) For strong skin surface clutter suppression, the advanced SSR scheme is introduced, where the frequency dependency of reflection waveform due to mutual coupling or near-field effect, has been accurately compensated by the FD model.
- 3) Clinical data over 100 subjects have been investigated in evaluating the proposed recognition scheme, where 3 - 9GHz band UWB MIMO radar module has been employed. Over those evaluations, our original SSR scheme offers more accurate recognition rate, compared to the case without the SSR process.

## II. SKIN SURFACE REJECTION(SSR)

### A. Observation Model

Fig. 1 shows the observation model, including the breast media. Multiple transmitter and receiver elements located at  $\mathbf{r}_T$  and  $\mathbf{r}_R$ , respectively, which rotates along the center of the breast.  $s(t, \theta; \mathbf{r}_T, \mathbf{r}_R)$  denotes the reflection signals at the combination of  $\mathbf{r}_T$  and  $\mathbf{r}_R$  with rotation angle  $\theta$ .

It is also assumed that the breast medium consists primarily of skin, adipose tissue, and fibroglandular tissue with dispersive and isotropic dielectric profiles.

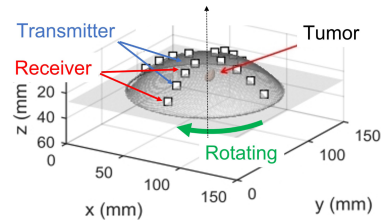


Fig. 1. Observation model. Multiple transmitter/receiver elements configure circular array, which is rotated along the vertical axis.

### B. Skin Surface Rejection (SSR) Method

In the context of cancer detection, it is essential to effectively eliminate skin surface reflections during pre-processing, as the signal strength of these reflections is significantly greater than that of the cancerous response. Otherwise, the stronger reflections can obscure the cancerous responses in the radar image. Various SSR methods have been developed to tackle this issue, with one commonly used approach being reference signal-based matching.

Notably, if the distance between the skin and antenna remains constant during array rotation, the subsequent averaging operation generates the reference signal  $\bar{s}_{\text{ref}}(t; \mathbf{r}_T, \mathbf{r}_R)$  with enhanced signal-to-noise ratio as follows:

$$\bar{s}_{\text{ref}}(t; \mathbf{r}_T, \mathbf{r}_R) = \frac{1}{N_\theta} \sum_{i=1}^{N_\theta} s(t, \theta_i; \mathbf{r}_T, \mathbf{r}_R) \quad (1)$$

where  $\theta_i$  denotes the  $i$ -th rotation angle and  $N_\theta$  is the total number of sampled rotation angles. Then, time-shift and amplitude adjustment has been determined as follow:

$$(\hat{A}, \hat{\tau}) = \underset{(A, \tau)}{\text{arg min}} \int_{T_r}^{T_r + T_w} |s(t, \theta; \mathbf{r}_T, \mathbf{r}_R) - A \bar{s}_{\text{ref}}(t - \tau; \mathbf{r}_T, \mathbf{r}_R)|^2 dt, \quad (2)$$

Here,  $T_r$  represents the rise time of  $s(t, \theta; \mathbf{r}_T, \mathbf{r}_R)$ , which can be determined by the peak of the cross-correlation functions between  $\bar{s}_{\text{ref}}(t; \mathbf{r}_T, \mathbf{r}_R)$  and  $s(t, \theta; \mathbf{r}_T, \mathbf{r}_R)$ .  $T_w$  denotes the temporal window length, that is determined by the effective pulse width of the transmitted signal. If  $T_w$  is either too short or too long relative to the effective pulse width, it can lead to under- or over-suppression, where the signals from fibroglandular or cancerous tissues may also be inadvertently suppressed. Using the optimized parameters for time-shift  $\hat{\tau}$  and amplitude  $\hat{A}$ , the reflection responses from the skin are subtracted as:

$$\tilde{s}_{\text{AVE}}(t, \theta; \mathbf{r}_T, \mathbf{r}_R) = s(t, \theta; \mathbf{r}_T, \mathbf{r}_R) - \hat{A} \bar{s}_{\text{ref}}(t - \hat{\tau}; \mathbf{r}_T, \mathbf{r}_R) \quad (3)$$

We call the above SSR scheme as SSR-AVE, for simplicity. While this approach relies on a simple process, it overlooks the frequency dependency of reflection response, which it typically caused by a mutual coupling or variations in the skin surface.

To address the above issue, the former study [33] introduced the FD model as the most effective suppression scheme. The advantage of introducing this method lies in its ability to account for the frequency dependency of the reflection signal, which is

influenced by mutual coupling effects or near-field effect. The FD-based reflection signal model is formulated as:

$$\tilde{s}_{\text{ref}}(t, \alpha; \mathbf{r}_T, \mathbf{r}_R) = \mathcal{F}^{-1} [(j\omega)^\alpha \bar{S}_{\text{ref}}(\omega; \mathbf{r}_T, \mathbf{r}_R)] \quad (4)$$

where  $\bar{S}_{\text{ref}}(\omega; \mathbf{r}_T, \mathbf{r}_R)$  is the frequency domain reference signal of  $\tilde{s}_{\text{ref}}(t, \mathbf{r}_T, \mathbf{r}_R)$ . The FD operator is denoted by the term  $(j\omega)^\alpha$ , where  $\alpha$  is so-called FD parameter.

In the SSR-FD scheme, the three parameters  $(A, \tau, \alpha)$  are optimized for each reflection response as follows:

$$\begin{aligned} (\hat{A}, \hat{\tau}, \hat{\alpha}) = \arg \min_{(A, \tau, \alpha)} \int_{T_r}^{T_r + T_w} & |s(t, \theta; \mathbf{r}_T, \mathbf{r}_R) \\ & - A \tilde{s}_{\text{ref}}(t - \tau, \alpha; \mathbf{r}_T, \mathbf{r}_R)|^2 dt, \end{aligned} \quad (5)$$

Then, the subtraction signal with SSR-FD is expressed as:

$$\begin{aligned} \tilde{s}_{\text{FD}}(t, \theta; \mathbf{r}_T, \mathbf{r}_R) = & s(t, \theta; \mathbf{r}_T, \mathbf{r}_R) \\ & - \hat{A} \tilde{s}_{\text{ref}}(t - \hat{\tau}, \hat{\alpha}; \mathbf{r}_T, \mathbf{r}_R) \end{aligned} \quad (6)$$

The template matching process described above primarily optimizes  $(\tau, A, \alpha)$  to minimize residuals between the observed and mathematically modeled signals. Notably, (2) and (5) need a non-linear optimization algorithm, in this case, we employ the simplex method [39], initializing the parameters as  $(\tau, A, \alpha) = (T_r, 1, 0)$ . Notably, the FD adjustments in (4) can compensate the frequency dependency of the skin reflection waveform, which cannot be achieved by simply time-shifting or amplitude adjustment.

### C. SVM Based Recognition

As one of the most promising and prevailed machine learning scheme, this study introduces the SVM based recognition. The SVM is one of the non-linear classification scheme, where the multi-dimensional input data are classified in the hyper-space using non-linear conversion. To reduce a computational complexity in non-linear conversion, the SVM introduces the following kernel function to measure the distance between the input vectors in hyper-space:

$$K(\mathbf{x}_i, \mathbf{x}_j) = \phi(\mathbf{x}_i)^\top \phi(\mathbf{x}_j) \quad (7)$$

where  $\phi(*)$  denotes the non-linear conversion operator. Here, we use the Gaussian kernel function as:

$$K(\mathbf{x}_i, \mathbf{x}_j) = \exp\left(-\frac{\|\mathbf{x}_i - \mathbf{x}_j\|^2}{2\sigma^2}\right) \quad (8)$$

where  $\sigma$  denotes the standard deviation in Gaussian function.

### D. Dimension Reduction of Input Vectors

To avoid an over-fitting issue in the machine learning process using a limited number of training data, the dimension reduction of the input vector is essential. Here, we introduce the following two dimension reduction schemes: Let the matrix  $\mathbf{Y} \in C^{M \times N}$  the complex scattered data of  $S(\omega, \theta; \mathbf{r}_T, \mathbf{r}_R)$ , where the SSR processing is completed in (3) or (6).  $N$  and  $M$  denote the number of frequency and rotation angle samples, respectively.

At first, the simple averaging (SA) based dimension reduction, defines the input vector  $\mathbf{X}^{\text{SA}} \in C^{1 \times N}$  as:

$$X_i^{\text{SA}} = \frac{1}{M} \sum_j Y_{i,j}, (i = 1, \dots, N) \quad (9)$$

The other scheme is the SVD based reduction as:

$$\mathbf{Y} = \mathbf{U}\mathbf{\Sigma}\mathbf{V} \quad (10)$$

where  $\mathbf{U}$  and  $\mathbf{V}$  denote the left and right singular vectors, respectively. Then, the compressed input vector is defined as  $\mathbf{X}^{\text{SVD}} = \mathbf{\Sigma}_{\text{max}} \mathbf{V}$ , where  $\mathbf{\Sigma}_{\text{max}}$  corresponds to the matrix with the largest singular value. Note that, it is expected that the SVD provides more noise-robust feature, by extracting the singular vector with the maximum singular values, where noise-components are effectively eliminated. Additionally, by compressing the data along the rotation angle, the SVD-based scheme efficiently extracts cancer response information even when the tumor position is deviated from the center of the breast, as cancer response strength depends on the rotation angle. Subsequently, by effectively capturing the cancer response though SVD, this approach minimizes accuracy variations caused by differences in tumor positioning. Fig. 2 presents the schematic illustration of the proposed method. Notably, principal component analysis (PCA) based dimensionality reduction has been applied in several studies [40], as an alternative compression scheme. In these applications, PCA performs eigenvalue decomposition on the covariance matrix of the signals. Meanwhile, SVD directly decomposes the original signal. However, several studies indicate that the differences between SVD- and PCA-based compression are not significant [41]. Therefore, we focus solely on SVD-based compression in the following analysis.

### E. Processing Flow of Proposed Method

The actual procedure of the proposed method is described as follows.

- Step 1): Reflection responses  $s(t, \theta_i; \mathbf{r}_T, \mathbf{r}_R)$  are processed by each SSR scheme in (3) or (6).
- Step 2): The dimension reduction is applied to the SSR processed responses  $\tilde{s}(t, \theta_i; \mathbf{r}_T, \mathbf{r}_R)$  using SA or SVD schemes in (9) or (10), and the input vector  $\mathbf{X} \in C^{1 \times N}$  is calculated for training data.
- Step 3): The SVM based supervised learning is carried out using a training dataset.
- Step 4): For each test data, Step 1) and 2) are applied, and the trained SVM classifies the input data as with or without cancer.

## III. CLINICAL TESTS AND DISCUSSIONS

### A. Measurement and Clinical Setup

The performance evaluation was conducted using clinical test data obtained from Hiroshima University Hospital. This clinical trial was conducted with written informed consent from the participants, which was approved by the Institutional Review Board of Hiroshima University Hospital. All procedures followed the

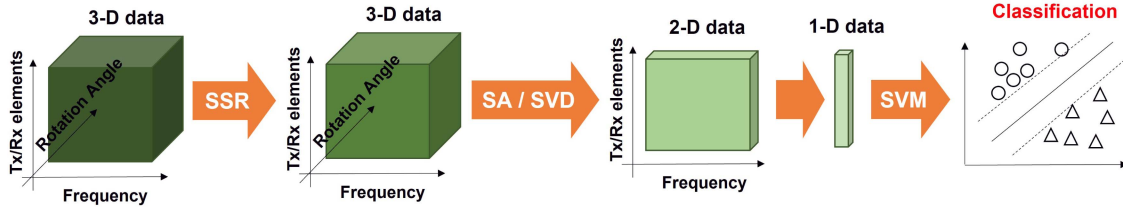
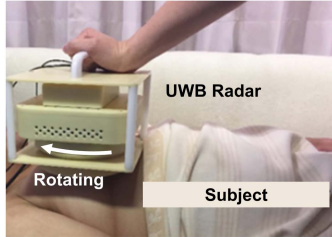


Fig. 2. Schematic illustration of the proposed classification scheme. Multiple transmitter/receiver elements configure circular array, which is rotated along the vertical axis.



(a) Measurement scene

Fig. 3. Measurement scene in clinical investigations in [15].

TABLE I  
NUMBER OF SUBJECTS AND BREAST DATA WITH OR WITHOUT TUMORS  
SELECTED BY THE SSR PERFORMANCE SELECTION ( $F_{\text{sup}} \leq 0.1$ )

	w/o tumor	w/ tumor
Number of breast data	27	37

guidelines outlined in the Japan Clinical Oncology Group Protocol Manual, version 2.6, which approves the breast cancer detection method and its measurement procedures, and is registered with the University Hospital Medical Information Network-Clinical Trials Registry under number UMIN000026181 [37].

The UWB handheld radar module, developed in [15], was used for the tests, which features a cross-shaped array of antennas, consisting of eight transmitters and eight receivers. This module repeatedly transmits a Gaussian-modulated mono-cycle pulse with a center frequency of 6.0GHz and a bandwidth of 6.7 GHz, *i.e.*, the operating frequency band is from 2.65 GHz to 9.35 GHz.

The array is positioned on a hemispheric dome with a radius of 76 mm, which is rotated from 0 to 360 degrees in  $45^\circ$  increments. Each antenna is a planar slot UWB antenna with the dimension of  $11 \text{ mm} \times 13.1 \text{ mm} \times 0.635 \text{ mm}$ , and the gain, directivity, and frequency characteristics of these antennas have been described in [38]. To ensure proper contact with the breast surface, this radar array is designed with a deep hole to accommodate the nipple, minimizing impedance mismatch between the air and breast, thus, a coupling medium is not used in this case. Fig. 3 shows the examination scene, using this hand-held radar module. Table I also provides details on the number of subjects with and without tumorous tissue, with both sides of the breast examined. For subjects with tumors, two distinct data sets were collected one from the breast with the tumor and one from the breast without it. This yielded a total of 131 clinical data sets with

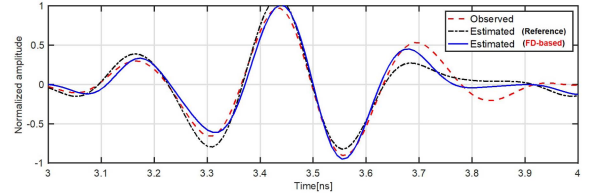


Fig. 4. Reflection responses. Red broken line is the measured signal. Black broken and blue solid lines are the reconstruction response of surface reflection using a reference and FD-based method, respectively.

tumors and 89 without, with diagnoses confirmed by a medical expert examining MRI or PET images

### B. Results of SSR

First, we investigate the efficacy of SSR approaches. Fig. 4 shows one example of a reflection response without and with SSR for the breast with tumor using each method. This figure demonstrated that the FD-based SSR method could compensate for the frequency dependency of the reflection response, particularly at the early time of peak responses between 3.3 and 3.6ns, which should not be a response from the tumor or other internal tissue.

In this clinical validation, we extract the samples, where the skin surface reflection is sufficiently eliminated. In order to quantitatively evaluate the SSR performance, the following metrics  $F_{\text{sup}}$  is introduced as:

$$F_{\text{sup}} = \frac{\max_{T_r \leq t \leq T_r + w} s_{\text{wSSR}}(t)}{\max_{T_r \leq t \leq T_r + w} s_{\text{woSSR}}(t)} \quad (11)$$

where  $s_{\text{woSSR}}(t)$  and  $s_{\text{wSSR}}(t)$  denote the signals without and with the SSR process, respectively, and  $0 \leq F_{\text{sup}} \leq 1$  holds. Fig. 5 shows the cumulative distribution function (CDF) of  $F_{\text{sup}}$  in each SSR method. This result demonstrates that the SSR FD method considerably reduces the  $F_{\text{sup}}$  value, compared with that obtained by the SSR AVE method, referring the constant CDF. In particular, the number satisfying  $F_{\text{sup}} \leq 0.1$  by the SSR FD (64) is 1.7 times larger than that by SSR AVE (37). Consequently, we extract the samples that satisfy  $F_{\text{sup}} \leq 0.1$  in the SSR-FD process, namely, 64 samples, for further recognition stage, where 37 samples with cancer and 27 samples without cancer as shown in Table I. Notably, the strength of skin reflection signals is significantly higher than that of internal tissue signals. Some studies have reported that the signal strength ratio of cancer to skin reflections is 1:10 [33], [36]. Thus, we selected

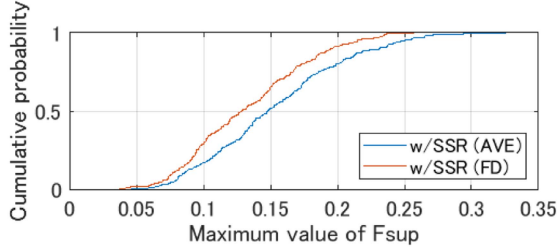


Fig. 5. Cumulative distribution function (CDF) for maximum value of  $F_{\text{sup}}$ . Blue and red curves denote the  $F_{\text{sup}}$  calculated by SSR-AVE and SSR-FD process.

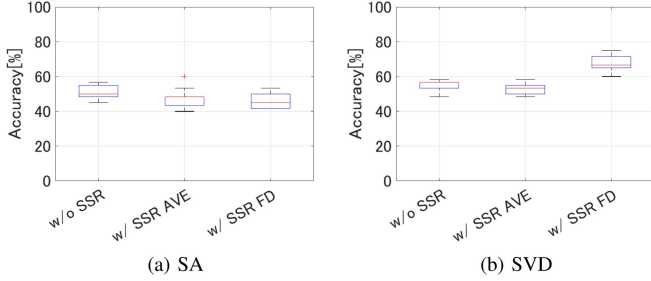


Fig. 6. Box plots of accuracy with or without using the SSR process for SA or SVD based dimension reduction schemes. Red line shows the median values. Box denotes the IQR.

datasets satisfying  $F_{\text{sup}} \leq 0.1$  to ensure effective suppression of skin reflections.

### C. SVM Classification

1) *Parameter Setting*: Next, the tumor recognition results by the SVM based classification. Here, we investigate the recognition accuracy by the SVM, in using each SSR scheme. At first, in order to generate the data matrix as  $Y$ , we extract 12 samples from 2.1GHz to 4.4GHz with 0.2GHz spacing. This frequency range is lower than the central frequency, which helps maintain a higher SNR by mitigating penetration loss. Specifically, using a lower frequency enhances the response from deeply embedded cancerous tissue compared to higher-frequency components. We evaluate 64 samples, and the 10 folds cross-validation scheme is introduced in the SVM based training.

Here, the accuracy is defined as  $\frac{\text{TP}+\text{TN}}{\text{TP}+\text{FP}+\text{TN}+\text{FN}}$ , where TP, FP, TN, and FN are the number of true positive, false positive, true negative, and false negative, respectively. Note that, the SVM learning process includes some randomly changed parameters in the optimization process, then, we take a median value for the accuracy in each sample with 10 times trials.

2) *Classification Result*: Fig. 6 shows the box plots for cases with or without using the SSR processing, where the SA or SVD based dimension reduction schemes in (9) or (10) are introduced. Here, each sample in the accuracy is determined by 64 classification results, which are averaged over 10 times trials in the SVM training. As shown in Fig. 6, while there are not significant difference among the SSR process in using the SA process, there are clear advantages for the SSR process in using

TABLE II  
MEDIAN AND IQR VALUES FOR CLASSIFICATION ACCURACY USING EACH CASE

Median [%] (IQR [%])	SA	SVD	CNN	
			Temporal	Frequency
w/o SSR	50.0 (6.7)	56.7 (3.3)	76.0 (43.0)	78.0 (52.0)
w/ SSR(AVE)	48.3 (5.0)	53.3 (5.0)	76.0 (52.0)	74.0 (50.0)
w/ SSR(FD)	45.0 (8.3)	66.7 (6.7)	50.0 (27.0)	52.0 (42.0)

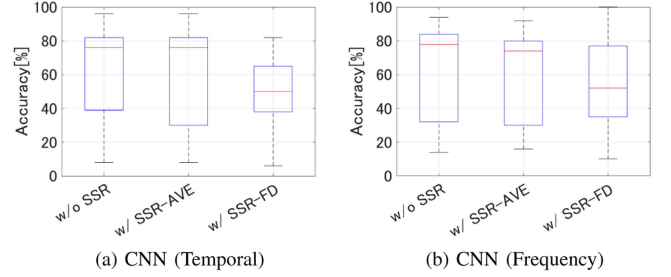


Fig. 7. Box plots of accuracy with or without using the SSR process for CNN based classification with temporal or frequency sinogram data. Red line shows the median values. Box denotes the IQR.

the SVD dimension reduction. Table II also summarizes the median values interquartile range (IQR) of classification accuracy for each condition, and demonstrates that the combination use of w/ SSR (FD) and SVD based input data compression provides the highest accuracy with small IQR among other combinations. In particular, the SVD based compression mainly contributes to an accuracy improvement, where the dominant components, being invariant to the rotation, can be well retrieved by using the SVD.

Notably, the accuracies in all approaches still remain less than 70 %, even in using the SSR-FD and SVD processes. This is caused by non-negligible responses from fibro-glandular tissues, which has the same level of dielectric parameters of the cancer tissue.

To validate the relevance of the proposed scheme, other deep-learning classification methods based on the CNN framework are investigated. Specifically, temporal and frequency sinograms without data compression along the rotation axis were used, as in [42] and [43], respectively. In the CNN scheme, the rotation variances of signals are effectively mitigated through convolution and pooling layers, and this action corresponds to the dimensionality reduction assumed in the proposed method (SA or SVM).

Fig. 7 presents a boxplot of the recognition accuracy achieved by CNN-based classification using both temporal and frequency sinogram data from the same dataset (64 samples). Meanwhile, Table II displays the median accuracy and IQR for each SSR scheme. While the CNN scheme without SSR or with SSR-AVE maintains relatively higher median accuracy values, its IQR is significantly larger than that of SVM-based results. This implies that SVM-based classification offers more stable recognition than the CNN approach.

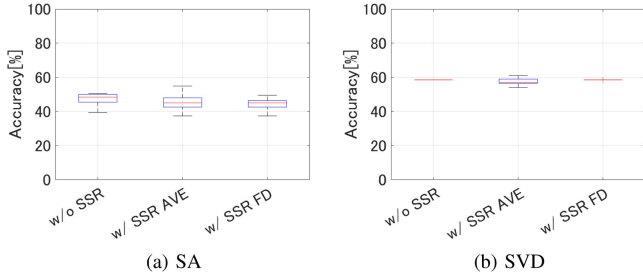


Fig. 8. Box plots of accuracy with or without using the SSR process for SA or SVD based dimension reduction schemes, where the data samples satisfying  $F_{\text{sup}} \leq 0.2$  are used (200 samples). Red line shows the median values. Box denotes the IQR.

TABLE III  
MEDIAN AND IQR VALUES FOR CLASSIFICATION ACCURACY DATA SAMPLES  
SATISFYING  $F_{\text{sup}} \leq 0.2$

Median [%] (IQR [%])	SA	SVD
w/o SSR	48.5 (4.5)	58.0 (0.0)
w/ SSR(AVE)	45.0 (5.5)	57.0 (2.5)
w/ SSR(FD)	45.0 (4.0)	58.5 (0.0)

We also investigate cases with different  $F_{\text{sup}}$  thresholds. As outlined in Section III-B, we selected a dataset satisfying  $F_{\text{sup}} \leq 0.1$ , comprising 64 samples. However, this dataset may provide insufficient samples for training, posing a potential risk of over-fitting. To address this, we increase the dataset size by relaxing the threshold to  $F_{\text{sup}} \leq 0.2$ , extracting 200 samples (117 samples with cancer and 83 samples without cancer). Fig. 8 presents a boxplot of the classification accuracy achieved by the SVD scheme, while Table III summarizes the median and IQR values for each case. Comparing the results presented in Fig. 6 and Table II, we observe significant differences are observed between datasets with  $F_{\text{sup}} \leq 0.1$  and  $F_{\text{sup}} \leq 0.2$ , particularly in relation to the proposed combination of SSR-FD and SVD processes (as seen in Figs. 6-(b) and 8-(b) and Tables II and III). For datasets where  $F_{\text{sup}} \leq 0.1$ , the SSR-FD and SVD processes achieve the highest accuracy, with a median value of 66.7 % (Q1: 65.0 %, Q3: 71.7 %). By contrast, for the dataset with  $F_{\text{sup}} \leq 0.2$ , the accuracy remains below 60 %, with a median value of 58.5 % (Q1 = Q3: 58.5 %). This finding clearly shows that the SSR performance significantly affects recognition accuracy. In addition, although increasing the number of training samples (200 samples under  $F_{\text{sup}} \leq 0.2$ ) typically enhances recognition accuracy in general machine learning tasks, this improvement is not observed when compared to the case of  $F_{\text{sup}} \leq 0.1$ . This suggests that expanding the dataset to include higher  $F_{\text{sup}}$  cases does not necessarily lead to better recognition accuracy. Because the  $F_{\text{sup}}$  value can be calculated without prior knowledge of skin position or reflection intensity, it serves as an indicator of the confidence level in the recognition results.

Notably, while transfer learning and regularization techniques can mitigate overfitting, they present challenges such as selecting an appropriate pre-trained network and determining regularization criteria (e.g., sparseness or statistical constraints) based on prior knowledge. Therefore, increasing the number of independent datasets is essentially required for further improving classification accuracy.

#### D. Discussions and Limitations

As evidenced by the above evaluations, the final recognition accuracy (approximately below 70 %) achieved using the proposed scheme remains inadequate for practical application. This is primarily attributed to the difficulty in distinguishing cancer responses from fibro-glandular tissue responses in the selected clinical datasets. Even with advanced deep-learning techniques such as CNNs (Fig. 7), accurately detecting cancer remains a significant challenge, highlighting the complexity of this classification task.

Additionally, refining the labeling process, such as by categorizing data based on tumor size and malignancy or incorporating prior information like mammary gland density, may further enhance the reliability of results and improve the generalizability of the proposed method. Moreover, the classification scheme used in this study relies on a binary decision (presence or absence of cancer). However, for practical applications, implementing a machine learning approach capable of providing a probabilistic quantitative index is essential. Such an approach would enhance method interpretability for medical professionals, enabling more nuanced decision-making, and improve reliability in real-world scenarios.

The primary contribution of this study lies in demonstrating that introducing a highly accurate SSR-FD scheme significantly enhances identification accuracy compared to cases without SSR or with SSR-AVE in SVM-based classification. These schemes are essential for extracting internal tissue responses while suppressing clutter (skin) reflections. These findings represent a notable practical advantage and make a meaningful contribution to the field, particularly in advancing signal processing techniques for microwave breast cancer diagnosis.

#### IV. CONCLUSION

This paper presented the back-scattered data based cancer recognition scheme, using an efficient skin clutter rejection scheme, known as SSR-FD, for microwave breast cancer diagnosis. As a promising SSR scheme, the FD based SSR approach has been introduced to suppress a skin reflection wave, even when distorted by frequency characteristic due to mutual coupling or near-field effect. In addition, the SVD based dimension reduction scheme has been developed to retain essential information in the rotating array observation model for the post-SVM based machine learning classification. The clinical data demonstrated that the SSR-FD has a significant superiority to the average based traditional SSR scheme, and the SVD dimension reduction scheme also contributes to the accuracy improvement, particularly when using the lower-frequency data.

Nonetheless, the available recognition accuracy (less than 70 %) is not sufficient to be applied in a practical scenario, and it should be incorporated with other schemes, such as permittivity estimation of breast via the tomography approach such as in [44].

## REFERENCES

- [1] F. Bray, J. Ferlay, I. Soerjomataram, R. L. Siegel, L. A. Torre, and A. Jemal, "Global cancer statistics 2018: GLOBOCAN estimates of incidence and mortality worldwide for 36 cancers in 185 countries," *CA, Cancer J. Clinicians*, vol. 68, no. 6, pp. 394–424, Dec. 2018.
- [2] L. Kranold, M. Taherzadeh, F. Nabki, M. Coates, and M. Popović, "Microwave breast screening prototype: System miniaturization with IC pulse radio," *IEEE J. Electromagn., RF Microw. Med. Biol.*, vol. 5, no. 2, pp. 168–178, Jun. 2021.
- [3] L. Fortaleza and M. Popović, "Narrowband microwave breast screening: Repeatability study with phantoms," *IEEE J. Electromagn., RF Microw. Med. Biol.*, vol. 6, no. 2, pp. 260–266, Jun. 2022.
- [4] M. Lazebnik et al., "A large-scale study of the ultrawideband microwave dielectric properties of normal, benign and malignant breast tissues obtained from cancer surgeries," *Phys. Med. Biol.*, vol. 52, pp. 6093–6115, 2007.
- [5] P. M. Meaney, M. W. Fanning, D. Li, S. P. Poplack, and K. D. Paulsen, "A clinical prototype for active microwave imaging of the breast," *IEEE Trans. Microw. Theory Techn.*, vol. 48, no. 11, pp. 1841–1853, Nov. 2000.
- [6] P. M. Meaney et al., "Initial clinical experience with microwave breast imaging in women with normal mammography," *Academic Radiol.*, vol. 14, no. 2, pp. 207–218, 2007.
- [7] D. O'Loughlin, M. O'Halloran, B. M. Moloney, M. Glavin, E. Jones, and M. A. Elahi, "Microwave breast imaging: Clinical advances and remaining challenges," *IEEE Trans. Biomed. Eng.*, vol. 65, no. 11, pp. 2580–2590, Nov. 2018.
- [8] E. Porter, M. Coates, and M. Popović, "An early clinical study of time-domain microwave radar for breast health monitoring," *IEEE Trans. Biomed. Eng.*, vol. 63, no. 3, pp. 530–539, Mar. 2016.
- [9] E. Porter and D. O'Loughlin, "Pathway to demonstrating clinical efficacy of microwave breast imaging: Qualitative and quantitative performance assessment," *IEEE J. Electromagn., RF Microw. Med. Biol.*, vol. 6, no. 4, pp. 439–448, Dec. 2022.
- [10] A. G. Dagheyan, A. Molaei, R. Obermeier, A. K. Martinez, and J. M. Lorenzo, "Near-field radar microwave imaging as an add-on modality to mammography," in *New Perspectives in Breast Imaging*. London, U.K.: IntechOpen, 2017, pp. 15–43.
- [11] G. Tiberi et al., "Evaluation of receiver operating characteristic curves in a microwave apparatus for breast lesions detection," in *Proc. Photonics Electromagn. Res. Symp.*, 2019, pp. 935–939.
- [12] L. Sani et al., "Breast lesion detection through MammoWave device: Empirical detection capability assessment of microwave images parameters," *PLoS One*, vol. 16, no. 4, 2021, Art. no. e0250005.
- [13] D. Byrne, M. Sarafianou, and I. J. Craddock, "Compound radar approach for breast imaging," *IEEE Trans. Biomed. Eng.*, Vol. 64, no. 1, pp. 40–51, Jan. 2017.
- [14] J. Moll, T. Slanina, J. Stindl, T. Maetz, D. H. Nguyen, and V. Krozer, "Temperature-induced contrast enhancement for radar-based breast tumor detection at K-band using tissue mimicking phantoms," *IEEE J. Electromagn., RF Microw. Med. Biol.*, vol. 7, no. 3, pp. 251–257, Sep. 2023.
- [15] H. Song et al., "Detectability of breast tumor by a hand-held impulse-radar detector: Performance evaluation and pilot clinical study," *Sci. Reports*, vol. 7, 2017, Art. no. 16353.
- [16] E. J. Bond, X. Li, S. C. Hagness, and B. D. Van Veen, "Microwave imaging via space-time beamforming for early detection of breast cancer," *IEEE Trans. Antennas Propag.*, vol. 51, no. 8, pp. 1690–1705, Aug. 2003.
- [17] W. C. Chew and Y. M. Wang, "Reconstruction of two-dimensional permittivity distribution using the distorted born iterative method," *IEEE Trans. Med. Imag.*, vol. 9, no. 2, pp. 218–225, Jun. 1990.
- [18] J. D. Shea, P. Kosmas, S. C. Hagness, and B. D. Van Veen, "Three-dimensional microwave imaging of realistic numerical breast phantoms via a multiple-frequency inverse scattering technique," *Phys. Med.*, vol. 37, no. 8, pp. 4210–4226, Aug. 2010, doi: 10.1118/1.3443569.
- [19] F. Gao, B. D. Van Veen, and S. C. Hagness, "Sensitivity of the distorted born iterative method to the initial guess in microwave breast imaging," *IEEE Trans. Antennas Propag.*, vol. 63, no. 8, pp. 3540–3547, Aug. 2015.
- [20] K. Noritake and S. Kidera, "Boundary extraction enhanced distorted born iterative method for microwave mammography," *IEEE Antennas Wireless Propag. Lett.*, vol. 18, no. 4, pp. 776–780, Apr. 2019, doi: 10.1109/LAWP.2019.2902351.
- [21] Z. Gong, Y. Chen, Y. Ding, and H. Zhang, "Perspective: Microwave medical imaging using space-time-frequency a priori knowledge for health monitoring," *IEEE J. Electromagn., RF Microw. Med. Biol.*, vol. 8, no. 1, pp. 2–14, Mar. 2024.
- [22] P. M. van den Berg and A. Abubakar, "Contrast source inversion method: State of art," *Prog. Electromagn. Res.*, vol. 34, pp. 189–218, 2001, doi: 10.2528/PIER01061103.
- [23] H. Sato and S. Kidera, "ROI limited unknowns reduction-based contrast source inversion for microwave breast imaging," *IEEE Antennas Wireless Propag. Lett.*, vol. 19, no. 12, pp. 2285–2289, Dec. 2020.
- [24] H. Sato and S. Kidera, "Noise-robust microwave breast imaging applied to multi-frequency contrast source inversion," *IEEE J. Electromagn., RF Microw. Med. Biol.*, vol. 5, no. 2, pp. 187–193, Jun. 2021.
- [25] L. Li, L. G. Wang, F. L. Teixeira, C. Liu, A. Nehorai, and T. J. Cui, "DeepNIS: Deep neural network for nonlinear electromagnetic inverse scattering," *IEEE Trans. Antennas Propag.*, vol. 67, no. 3, pp. 1819–1825, Mar. 2019.
- [26] K. H. Jin, M. T. McCann, E. Froustey, and M. Unser, "Deep convolutional neural network for inverse problems in imaging," *IEEE Trans. Image Process.*, vol. 26, no. 9, pp. 4509–4522, Sep. 2017.
- [27] X. Ye, Y. Bai, R. Song, K. Xu, and J. An, "An inhomogeneous background imaging method based on generative adversarial network," *IEEE Trans. Microw. Theory Techn.*, vol. 68, no. 11, pp. 4684–4693, Nov. 2020.
- [28] Y. Zhou, Y. Zhong, Z. Wei, T. Yin, and X. Chen, "An improved deep learning scheme for solving 2-D and 3-D inverse scattering problems," *IEEE Trans. Antennas Propag.*, vol. 69, no. 5, pp. 2853–2863, May 2021.
- [29] Z. Wei and X. Chen, "Uncertainty quantification in inverse scattering problems with Bayesian convolutional neural networks," *IEEE Trans. Antennas Propag.*, vol. 69, no. 6, pp. 3409–3418, Jun. 2021.
- [30] J. E. Fajardo, J. Galvan, F. Vericat, C. Manuel Carlevaro, and R. M. Irastorza, "Phaseless microwave imaging of dielectric cylinders: An artificial neural networks-based approach," *Prog. Electromagn. Res.*, vol. 166, pp. 95–105, 2019.
- [31] Z. Wei and X. Chen, "Physics-inspired convolutional neural network for solving full-wave inverse scattering problems," *IEEE Trans. Antennas Propag.*, vol. 67, no. 9, pp. 6138–6148, Sep. 2019.
- [32] S. K. Davis, B. D. Van Veen, S. C. Hagness, and F. Kelcz, "Breast tumor characterization based on ultrawideband microwave backscatter," *IEEE Trans. Biomed. Eng.*, vol. 55, no. 1, pp. 237–246, Jan. 2008.
- [33] K. Noritake and S. Kidera, "Surface clutter suppression with FDTD recovery signal for microwave UWB mammography," *IEICE Trans. Electron.*, vol. E 103-C, no. 1, pp. 26–29, Jan. 2020.
- [34] F. Abujarad, A. Jostingmeier, and A. Omar, "Clutter removal for landmine using different signal processing techniques," in *Proc. Int. Conf. Ground Penetrating Radar*, 2004, pp. 697–700.
- [35] W. Zhi and F. Chin, "Entropy-based time window for artifact removal in UWB imaging of breast cancer detection," *IEEE Signal Process. Lett.*, vol. 13, no. 10, 585–588, Oct. 2006.
- [36] H. Song et al., "A two-stage rotational surface clutter suppression method for microwave breast imaging with multistatic impulse-radar detector," *IEEE Trans. Instrum. Meas.*, vol. 69, no. 12, pp. 9586–9598, Dec. 2020.
- [37] S. Sasada et al., "Portable impulse-radar detector for breast cancer: A pilot study," *Proc. SPIE*, vol. 5, no. 2, Apr. 2018, Art. no. 025502.
- [38] T. Sugitani, S. Kubota, M. Hafiz, X. Xiao, and T. Kikkawa, "Three-dimensional confocal imaging for breast cancer detection using CMOS Gaussian monocycle pulse transmitter and 4 x 4 ultra wideband antenna array with impedance matching layer," *Japanese J. Appl. Phys.*, vol. 53, no. 4S, Mar. 2014, Art. no. 04EL03.
- [39] G. K. Murty, *Linear Programming*, New York, NY, USA: Wiley, 1983.
- [40] S. S. Tilwankar and B. S. Kirar, "Breast cancer detection using principal component analysis and machine learning models," in *Proc. 1st Int. Conf. Adv. Comput. Future Commun. Technol.*, Meerut, India, 2021, pp. 80–84.
- [41] E. Muningsih et al., "Comparative analysis on dimension reduction algorithm of principal component analysis and singular value decomposition for clustering," *J. Phys., Conf. Ser.*, vol. 1641, 2020, Art. no. 012101.
- [42] T. Reimer and S. Pistorius, "The diagnostic performance of machine learning in breast microwave sensing on an experimental dataset," *IEEE J. Electromagn., RF Microw. Med. Biol.*, vol. 6, no. 1, pp. 139–145, Mar. 2022.

- [43] A. Ueda and S. Kidera, "Frequency sinogram based cancer recognition via convolutional neural network for microwave breast cancer diagnosis," *IEICE Trans. Commun.*, early access, Feb. 14, 2025, doi: [10.23919/transcom.2024EBP3146](https://doi.org/10.23919/transcom.2024EBP3146).
- [44] P. Zhu and S. Kidera, "Complex permittivity reconstruction using skin surface reflection and neural network for microwave breast imaging," *IEEE J. Electromagn., RF Microw. Med. Biol.*, vol. 7, no. 4, pp. 425–431, Dec. 2023.



**Ayumi Ueda** received the B.E. degree in electrical and electronic engineering from the Tokyo University of Science, Shinjuku, Japan, in 2023, and M.E degree from the Graduate School of Informatics and Engineering, The University of Electro-Communications, Tokyo, Japan in 2025. Her research interest includes signal processing, imaging, and deep learning approaches for microwave biomedical applications.



**Shouhei Kidera** (Senior Member, IEEE) received the B.E. degree in electrical and electronic engineering and the M.I. and Ph.D. degrees in informatics from Kyoto University, Kyoto, Japan, in 2003, 2005, and 2007, respectively. In 2009, he joined The University of Electro-Communications, Tokyo, Japan, as an Assistant Professor, where he is currently a Full Professor with the Graduate School of Informatics and Engineering, The University of Electro-Communications. His research interests include advanced radar signal processing, electromagnetic inverse scattering issue

for ultra wideband (UWB) three-dimensional sensor, and bio-medical applications. Since 2016, he has been with Cross-Disciplinary Electromagnetics Laboratory, The University of Wisconsin Madison, Madison, WI, USA, as a Visiting Researcher. He has been also the Principal Investigator of the PRESTO Program of Japan Science and Technology Agency from 2017 to 2021. He was the recipient of the 2012 Ando Incentive Prize for the Study of Electronics, 2013 Young Scientist's Prize by the Japanese Minister of Education, Culture, Sports, Science and Technology (MEXT), and 2014 Funai Achievement Award, 2022 KDDI Foundation Award, Contribution Award, and 2023 RIEC Award. He is a Senior Member of the Institute of Electronics, Information, and Communication Engineers of Japan, and the International Union of Radio Science (Union Radio-Scientifique Internationale, URSI), and a Member of the Institute of Electrical Engineering of Japan, and the Japan Society of Applied Physics.